NANO LETTERS

Letter

pubs.acs.org/NanoLett

Unraveling the High Open Circuit Voltage and High Performance of Integrated Perovskite/Organic Bulk-Heterojunction Solar Cells

Shiqi Dong,[†] Yongsheng Liu,[*,†,‡] Ziruo Hong,[†] Enping Yao,[†] Pengyu Sun,[†] Lei Meng,[†] Yuze Lin,[§] Jinsong Huang,[§] Gang Li,[†] and Yang Yang[*,†]

[†]Department of Materials Science and Engineering, University of California, Los Angeles, California 90095, United States

[‡]Key Laboratory of Functional Polymer Materials, Institute of Polymer Chemistry, College of Chemistry, Nankai University, Tianjin 300071, China

[§]Department of Mechanical and Materials Engineering and Nebraska Center for Materials and Nanoscience, University of Nebraska-Lincoln, Lincoln, Nebraska 68588, United States

Supporting Information

ABSTRACT: We have demonstrated high-performance integrated perovskite/bulk-heterojunction (BHJ) solar cells due to the low carrier recombination velocity, high open circuit voltage (V_{OC}), and increased light absorption ability in near-infrared (NIR) region of integrated devices. In particular, we find that the V_{OC} of the integrated devices is dominated by (or pinned to) the perovskite cells, not the organic photovoltaic cells. A Quasi-Fermi Level Pinning Model was proposed to understand the working mechanism and the origin of the V_{OC} of the integrated perovskite/BHJ solar cell, which following that of the perovskite solar cell and is much higher than that of the low bandgap polymer based organic BHJ solar cell. Evidence for the model was enhanced by examining the charge carrier behavior and photovoltaic behavior of the integrated devices under illumination of monochromatic light-emitting diodes at different characteristic wavelength. This finding shall pave an interesting possibility for integrated photovoltaic devices to harvest low energy photons in NIR region and further improve the current density without sacrificing V_{OC}, thus providing new opportunities and significant implications for future industry applications of this kind of integrated solar cells.

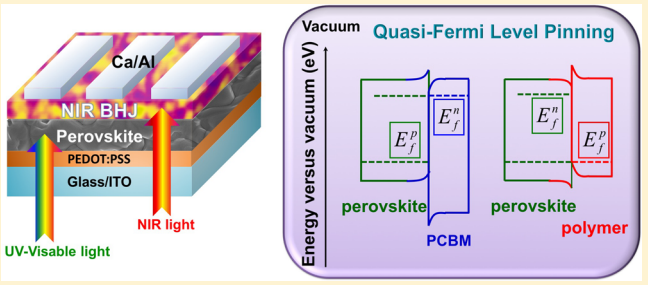

KEYWORDS: *Perovskite, photovoltaic, bulk heterojunction, Fermi level*

Metal halide based organic−inorganic hybrid perovskite solar cells have been attracting increasing attention in recent years due to the rapid progress in terms of increased efficiency.[1,2] It has become a promising next-generation photovoltaic technology due to its potential to be lightweight, mechanically flexible and manufactured in a cost-effective manner. The power conversion efficiency (PCE) of perovskite solar cells (PSC) has risen from 3.8% to over 20% in the past few years.[3−7] Such a rapid increase in efficiency is attributed to the unique physical properties of the organic−inorganic hybrid perovskite, such as the excellent light absorption coefficient, long exciton diffusion length, ambipolar transport properties, and low cost fabrication of large area devices.[8−10] In addition, the accumulated knowledge in the organic photovoltaic (OPV) and dye-sensitized solar cells (DSSC) also have played an important role in such rapid progress.[11−16]

Moreover, several perovskite-based photovoltaic device architectures, including both conventional and inverted architectures, have successfully demonstrated high PCE due to the intrinsic properties of perovskite materials.[17−20] Current organic−inorganic hybrid perovskite materials using organic cations, such as $CH_3NH_3^+$ or $NH_2CH{=}NH_2^+$, show an onset light response limited between 800 to 850 nm, which hinders near-infrared (NIR) light harvesting and thus further impedes PCE improvement. Thus, one important strategy to further enhance the photovoltaic performance of perovskite photovoltaic devices lies in broadening the light absorption to include the NIR region. To use the NIR part of the solar spectrum, tin halide-based low band gap perovskites, such as $CH_3NH_3SnI_3$, have been used as light harvesters for solar cell applications.[21,22] Although the onset photocurrent response in the light absorbing tin halide based perovskites extends to over 1000 nm, it is a challenge to further use these materials for future industry applications due to the poor Sn(II) stability and low PCE.[21−24] An even greater problem is that lowering the band gap will result in an smaller open circuit voltage (V_{OC}).[25] One of the main applications of low band gap polymers in solar cells is to fabricate tandem devices that better utilize the sunlight from the visible to NIR region. It has been reported that integrated perovskite/BHJ photovoltaic device is an efficient

Received: June 15, 2017
Revised: July 15, 2017
Published: July 20, 2017

DOI: 10.1021/acs.nanolett.7b02532
Nano Lett. 2017, 17, 5140−5147

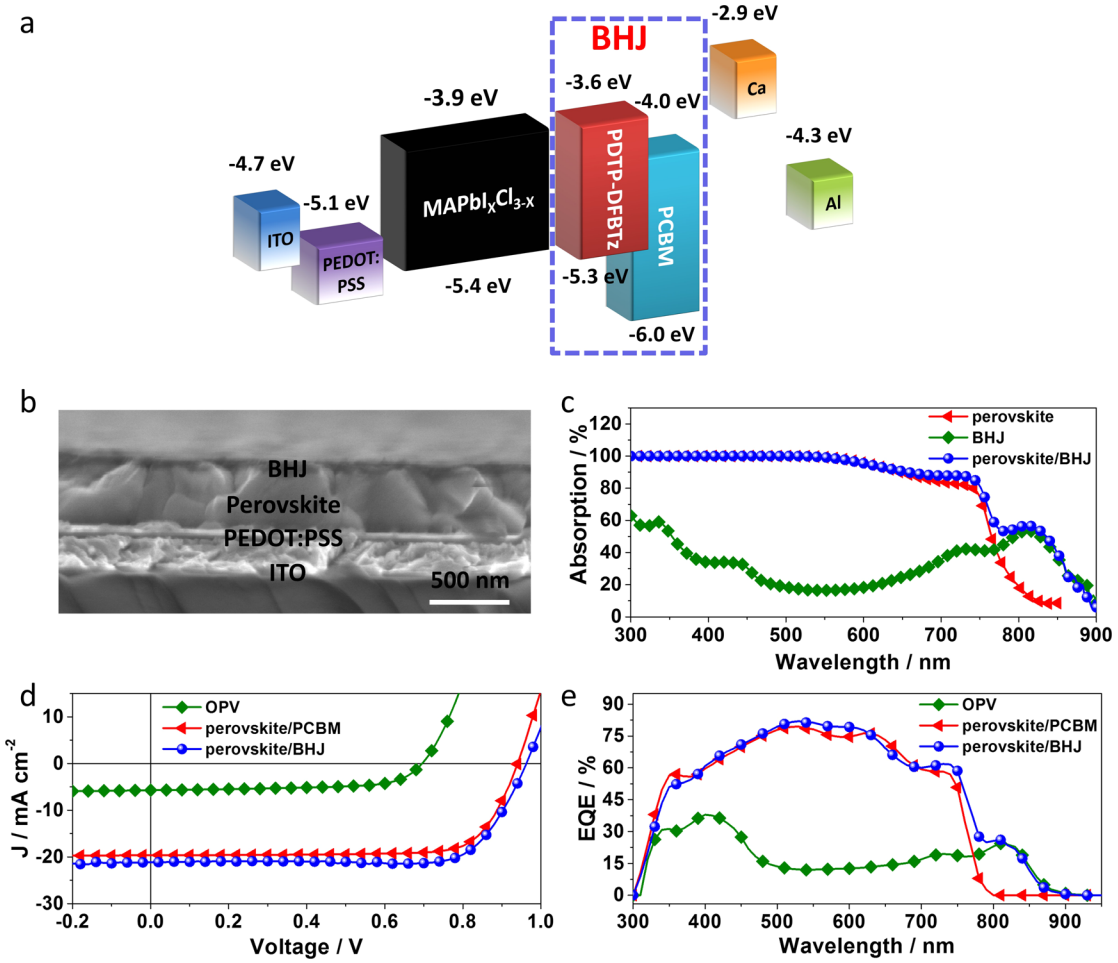

Figure 1. (a) Energy levels of the integrated perovskite/BHJ devices. (b) Cross-section SEM for the integrated device without metal electrode. (c) UV−vis-NIR absorption spectra of perovskite, BHJ, and perovskite/BHJ film. (d) Current density versus voltage (J−V) curves of OPV cell, regular, and integrated perovskite/BHJ solar cells. (e) EQE of the corresponding devices. The donor and acceptor used in the BHJ films are PDTP-DFBT and PCBM, respectively.

method to absorb sun light in the NIR region by combining the advantages of perovskite solar cells and NIR organic solar cells.[26−28] Considering the integrated photovoltaic device, which has two absorber layers directly in contact, similar to a tandem device but without a recombination layer (or a tunnel junction) in-between, the performance should be limited by the poorer performing material. Because electrons and holes recombine in the film during charge transport due to a lack of an interconnecting layer, it should not work like a conventional solar cell. However, the integrated perovskite/BHJ device works well in both conventional and inverted architectures.[26−28] Although the efficiency of the devices based on this perovskite/BHJ structure is still low and the working principles behind this device structure are poorly understood, this kind of device has shown promising advantages for further improving the performance of perovskite solar cells. Thus, further investigation is needed to understand the mechanism of the integrated cells.

In this work, we demonstrated an efficient integrated perovskite/BHJ device using PDTP-DFBT[29] as NIR polymer donor in BHJ layer. External quantum efficiency (EQE) data shows that the integrated devices exhibit an extended photoresponse into the near-infrared region up to 900 nm, which is unambiguously attributed to the photogeneration in NIR BHJ film. Note that the perovskite used in this work is $CH_3NH_3PbI_{3-x}Cl_x$. It is interesting to see that the V_{OC} of the integrated perovskite/BHJ device is preserved from the perovskite solar cell, and much higher than that of low band gap polymer based BHJ OPV cell. We use another low band gap polymer, PBDTT-DPP,[30] in BHJ film to further verify that the perovskite device, rather than the OPV device, dominates the V_{OC} of the integrated devices. Besides the biabsorption layers system in this work and our previous work, we found that the V_{OC} of integrated perovskite/BHJ solar cells reported by other groups also follows that of the pristine perovskite solar cell, the higher of the two in the bilayer structure, for reasons that were not clear.[26,27] To unveil the working principles and concretely understand the mechanism of this kind of device, we further analyze and explain the high V_{OC} based on the band structure. For the first time, a quasi-Fermi Level Pinning Model is proposed to explain the preserved high V_{OC} of the integrated perovskite/BHJ solar cell based on the band structure of such integrated device. Evidence for the pinning of quasi-Fermi levels was also presented following a series of carefully designed experiments. We note that the success of such energy level pinning should be attributed to the uniqueness of this perovskite/BHJ bilayer configuration and matched energy level between the perovskite with polymer and fullerene derivative. This finding suggests a novel direction for future photovoltaic device architecture and shall pave the way for

DOI: 10.1021/acs.nanolett.7b02532
Nano Lett. 2017, 17, 5140−5147

Table 1. Performance Parameters for Optimized Photovoltaic Devices Prepared with BHJ OPV Device, Regular Device (Perovskite/PCBM) and Integrated Device (Perovskite/BHJ)[a]

	V_{OC} (V)	J_{SC} (mA cm^{-2})	FF (%)	PCE (%)	decay time[b] (μs)	decay time[c] (μs)
OPV device	0.70	5.72	66	2.64 (2.54 ± 0.1)	0.67	1.03
regular device	0.94	19.6	77	14.2 (12.2 ± 2.0)	0.68	0.45
integrated device	0.96	21.1	78	15.8 (14.0 ± 1.8)	0.46	0.99

[a]The donor and acceptor used in the BHJ film are PDTP-DFBT and PCBM, respectively. [b]Decay time extracted from transient photocurrent measurement. [c]Decay time extracted from transient photovoltage measurement.

material selection to achieve even higher power conversion efficiency (PCE) due to the increased J_{SC} and the high preserved V_{OC}. Coupled with the diversity of low band gap conjugated polymers/oligomers and high photovoltaic performance, our findings shall provide new opportunities and significant implications for future industry applications of this kind of integrated solar cells.

Figure 1a shows the device structure and the energy band diagram of our integrated cell. The ambipolar charge transport properties of perovskite with high hole and electron carrier mobility play an important role in this integrated device. Following illumination, holes generated in the perovskite film will be extracted by PEDOT:PSS and transported to the anode. Concurrently, electrons generated in the perovskite film will be extracted by PCBM in the BHJ film and transport to the cathode. Here, the BHJ will also contribute photocurrent as excitons will be formed after absorbing the NIR part of the sunlight, and electron/hole carriers will be generated after separating at the donor/acceptor interface (like regular OPV cells). The holes generated in the BHJ film will transport through the polymer to the perovskite and then be extracted by PEDOT:PSS; meanwhile, the electrons generated in the BHJ film will transport through PCBM to the cathode. Note that because the HOMO level of the polymer (−5.3 eV) is nearly identical to that of the valence band (VB) of perovskite (−5.4 eV), a small barrier may form when holes generated in the BHJ move through the perovskite toward the anode. The cross-sectional SEM image of the integrated perovskite/BHJ device without a metal electrode is shown in Figure 1b, which confirms that the device configuration is a well-defined layer-by-layer structure. The BHJ layer is seen to uniformly cap the perovskite film, indicating an efficient protection to the perovskite layer. The thicknesses of the PEDOT:PSS, $CH_3NH_3PbI_{3-x}Cl_x$ and BHJ layers are ∼40, ∼360, and ∼65 nm, respectively. The absorption spectra (extracted from reflection spectrum (R%) by 100 − R) of perovskite, BHJ, and perovskite/BHJ films are shown in Figure 1c. The perovskite/BHJ film shows a very good solar spectral coverage from 300 to 900 nm, which is ascribed to the good combination of the absorption of perovskite and BHJ films.

Figure 1d presents the photocurrent density−voltage (J−V) curves of the integrated perovskite/BHJ devices with both a BHJ organic photovoltaic (OPV) device and a perovskite reference device for comparison. The detailed solar cell performance parameters are summarized in Table 1. Note that for comparison we use the same method to fabricate the BHJ layer and the BHJ thickness is similar in the single junction OPV device and integrated device. As shown in Figure 1d, the PDTP-DFBT:PCBM based BHJ OPV device exhibits a short circuit current density (J_{SC}) of 5.72 mA cm^{-2}, an open circuit voltage (V_{OC}) of 0.70 V and a fill factor (FF) of 66%, which yields a PCE of 2.64%. The reference perovskite photovoltaic device with PCBM as the ETL has a relatively low efficiency of 14.2%, coupled with a J_{SC} of 19.6 mA cm^{-2}, a V_{OC} of 0.94 V, and an FF of 77%. Blending the low band gap polymer PDTP-DFBT with PCBM to form the integrated perovskite/BHJ layer resulted in a J_{SC} of 21.1 mA cm^{-2}, a V_{OC} of 0.96 V, and an FF of 78%. Finally, the PCE increased to 15.8%. As can be seen, the enhancement in the PCE is mainly due to the increase in the J_{SC} and the high preserved V_{OC}. The thickness of the BHJ layer in the integrated device is about 60 nm. Further increasing the thickness will increase series resistance, leading to a reduction in FF, as show in Figure S2 (Supporting Information).

A very interesting and unusual observation is apparent when comparing the integrated device's V_{OC} to the regular perovskite and OPV's V_{OC}. The integrated device follows the V_{OC} (or even slightly higher V_{OC}) of the regular perovskite device. As discussed below, a slightly higher V_{OC} of the integrated device may be due to the reduced carrier recombination for the integrated device. Note that we further selected another low band gap polymer, PBDTT-DPP to verify that the perovskite device, rather than the OPV device, dominates the V_{OC} of the integrated devices, as show in Figure S3 and Table S1 (Supporting Information). The integrated perovskite/BHJ device using PBDTT-DPP as donor material shows a high V_{OC} of ∼0.95 V, which follows the V_{OC} of the regular perovskite device. The 0.95 V V_{OC} is much higher than that of PBDTT-DPP based BHJ OPV device (0.74 V).[30] The statistical data of regular perovskite solar cells and PDTP-DFBT based integrated perovskite/BHJ solar cells are shown in Figure S4 (Supporting Information). Accordingly, we found that the integrated devices exhibit slightly higher V_{OC}, J_{SC}, and comparable FF when compared to that of regular perovskite device. As a result, the integrated device had a greater PCE. Note that the related integrated photovoltaic devices show similar hysteresis in the J−V curves (Figure S5a and Table S1, Supporting Information) to regular perovskite devices.[31−33] The steady-state efficiency measured by holding a voltage at the maximum power point was also provided as a comparison for device performance (Figure S5b, Supporting Information).

EQE curves of the optimized integrated perovskite/BHJ device as well as single junction perovskite device and BHJ OPV device are shown in Figure 1e and J_{SC} values calculated from the integration of EQE curves over AM 1.5G solar spectrum are summarized in Table S2 (Supporting Information). As shown in Figure 1e, the BHJ OPV device using PDTP-DFBT as a donor shows a photocurrent response from 300 to 900 nm, which is consistent with its absorption spectra (Figure 1). The EQE of a conventional perovskite device shows the characteristic 300−800 nm absorption band of perovskite film. Meanwhile, the integrated perovskite/BHJ device shows a photoresponse up to 900 nm, which originates from the low band gap polymer BHJ film.

Besides the bilayer system in this work and our previous paper, we also find that the related work, although limited, done by other groups also shows the similar phenomenon, which is

DOI: 10.1021/acs.nanolett.7b02532
Nano Lett. 2017, 17, 5140−5147

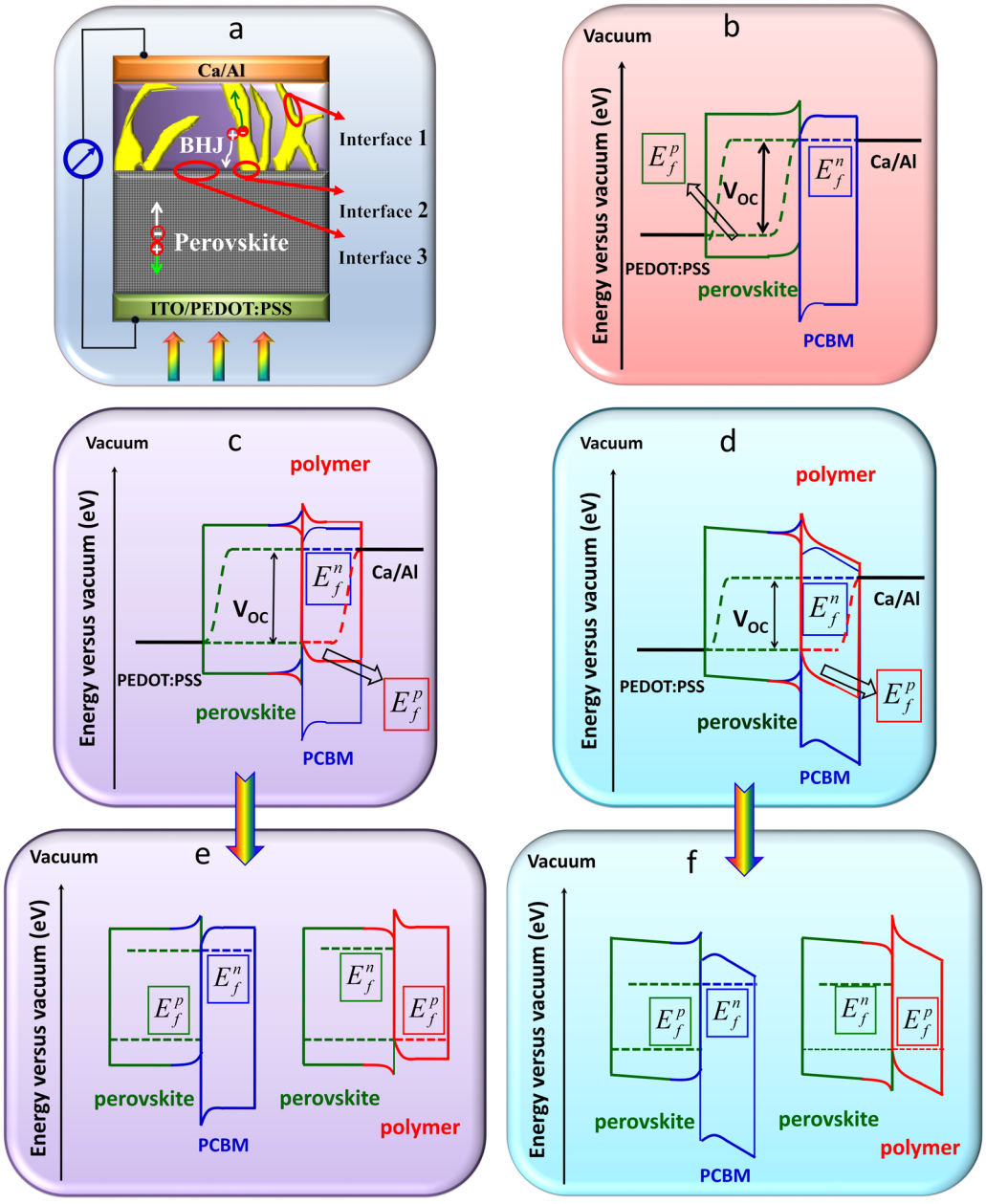

Figure 2. Energy band diagram of perovskite cell and perovskite/BHJ cell. (a) Charge generation and transport mechanism of the integrated device. (b) The quasi-Fermi level splitting in the perovskite layer when pure PCBM is the ETL layer. The quasi-Fermi level splitting in perovskite layer and BHJ layer in integrated perovskite/BHJ cells at (c) open circuit condition, and (d) maximum power point. Detailed band diagrams of electrons and holes of the perovskite/BHJ cells at (e) open circuit condition, and (f) maximum power point.

that the open circuit voltage of integrated perovskite/BHJ solar cell follows that of the pristine perovskite solar cell, the higher of the two in the bilayer structure.[27,28] Thus, we believe the high preserved V_{OC} of the integrated solar cell is not by accident but rather it must root from solid physical mechanism. For a typical single-junction solar cell, the upper limit for the open circuit voltage is determined by the quasi-Fermi level splitting of the solar cell absorber layer under steady-state illumination. In our integrated perovskite/BHJ biabsorption layer structure, the situation becomes more complicated because three heterojunctions coexist in one system. The simplified interfaces of polymer/PCBM, perovskite/PCBM and perovskite/polymer are illustrated and labeled as shown in Figure 2a. Upon illumination, each interface will produce a potential difference, which will contribute to the final open circuit voltage of the solar cell. As the polymer/fullerene interface has been extensively studied, we here focus on the interfaces between perovskite and the two components of the organic BHJ. We carefully examine the energy diagram, as shown in Figure 2, and figure out the physical origin of the open circuit voltage of the integrated devices.

In the energy diagrams in Figure 2, E_f^p and E_f^n represent the quasi-Fermi levels for holes and electrons, respectively. The quasi-Fermi level splitting in the perovskite layer when pure PCBM is the ETL is shown in Figure 2b as a reference. When exposed to sunlight, in the traditional heterojunction device structure consisting of two materials the E_f^p and E_f^n of these two materials have to be aligned simultaneously. However, in the BHJ system the electron-rich PCBM and the hole-rich polymer are two different materials which form the BHJ blend.

DOI: 10.1021/acs.nanolett.7b02532
Nano Lett. 2017, 17, 5140−5147

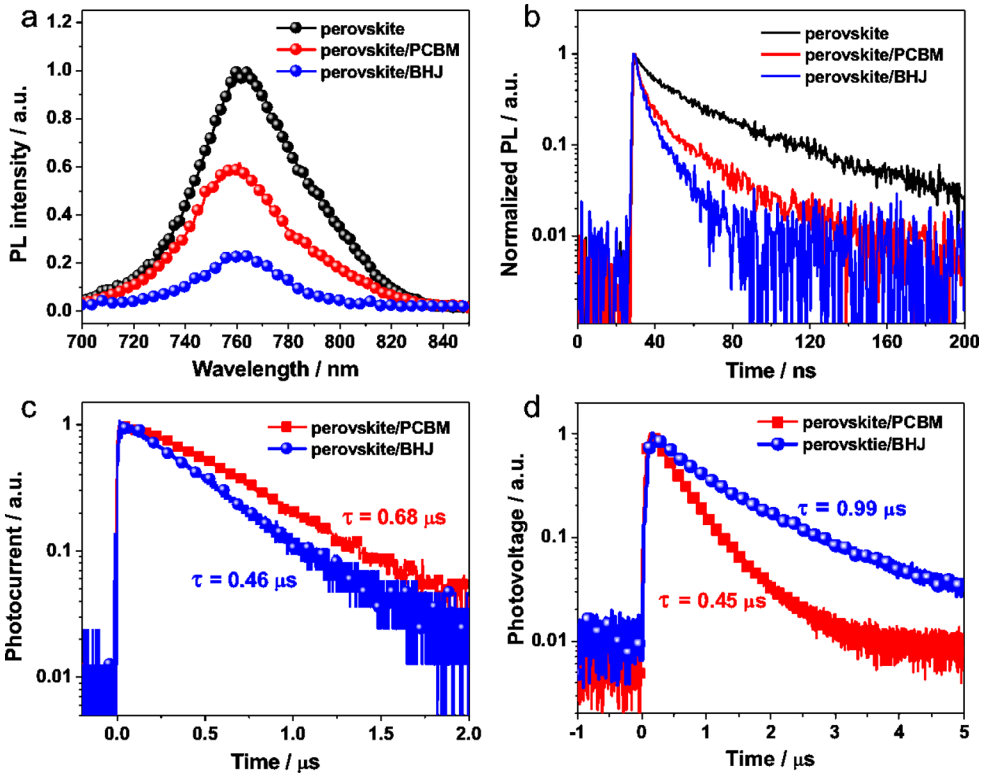

Figure 3. (a) The steady-state PL spectra and (b) time-resolved PL decay spectra of glass/perovskite ($CH_3NH_3PbI_{3-x}Cl_x$), glass/perovskite ($CH_3NH_3PbI_{3-x}Cl_x$)/PCBM and glass/perovskite ($CH_3NH_3PbI_{3-x}Cl_x$)/BHJ (PDTP-DFBT:PCBM). (c) Transient photocurrent decay curves of the regular device and integrated device. (d) Transient photovoltage decay curves of the regular device and integrated device.

Therefore, this unique system allows the perovskite's E_f^p to align with the polymer's E_f^p; in the meantime, the perovskite's E_f^n is allowed to align with the PCBM's E_f^n. This is illustrated in the Figure 2c for the open circuit condition and Figure 2d for the maximum-power condition, respectively. In Figure 2e,f, the detail alignment of E_f^p and E_f^n, respectively, are provided. The LUMO level of the PCBM (4.0 eV) is slightly lowered than the perovskite conduction band (3.9 eV), hence, the photoinduced electrons from the perovskite will diffuse to PCBM and cause the PCBM's band to bend upward when reaching equilibrium in the open circuit condition. On the other hand, the holes from the perovskite will also diffuse to polymer and cause the polymer's band to bend downward. The BHJ structure therefore has an "effective quasi Fermi-level" very similar to that of the perovskite's quasi-Fermi levels. This can only happen when the perovskite layer provides sufficient photogenerated charges to "pin" the quasi Fermi-levels in this integrated PV structure. In addition, the relative slow recombination velocity in the polymer:fullerene blend, also helps the integrated device to maintain its quasi-Fermi levels. Note that the slow recombination is evidenced in the charge dynamic study (Figure S8, Supporting Information). Because the V_{OC} output is closely related to the quasi-Fermi level splitting in a solar cell, therefore, the pinning of the quasi-Fermi level of our integrated device indeed allows this high V_{OC} of the perovskite to be preserved, while adding the NIR part of the photocurrent into the integrated device.

Figure 2d shows the band alignment of the maximum-power condition, which illustrates the operation of the device when it is wired to an external load. The slight tilt of the overall integrated device provides the driving force for the electron and holes to be extracted to the external circuits. It is noted that there is a smaller energy difference between the HOMO of the polymer and the valence band of the perovskite; because the difference is rather small (only ~0.1 eV), the holes should be able to tunnel through the small bend−bending at the interface between the perovskite and the polymer. This is consistent with our observation that the polymer contributes to photocurrent by ~1.5 mA cm^{-2}. On the other hand, we observed improved photocurrent due to the contribution from polymer:fullerene BHJ absorber layer.

To prove the hypothesis of quasi-Fermi Level pinning model, we prepared $CH_3NH_3PbI_{3-x}Cl_x$, $CH_3NH_3PbI_{3-x}Cl_x$/PCBM and $CH_3NH_3PbI_{3-x}Cl_x$/BHJ (PDTP-DFBT:PCBM) films on glass substrates and measured the steady-state photoluminescence (PL) of the three films using excitation of 640 nm laser. The steady-state PL of perovskite/PDTP-DFBT was also measured for comparison (Figure S7). As shown in Figure 3a, all three curves show the same photoluminescence peak, which indicates that the PL is determined by the bandgap of perovskite. Meanwhile, the PL quenching of BHJ film interfaced with perovskite is faster than that of PCBM film interfaced with perovskite, indicating faster charge carrier transfer from perovskite into the BHJ film. This means that the charge injection from perovskite to BHJ film is more efficient than to PCBM, and consequently the charge extraction is improved in the integrated device. We note that the concentration of PCBM in the polymer/PCBM solution is 8 mg/mL, which is lower than half of the PCBM concentration of pure PCBM solution (20 mg/mL) for PCBM transporting layer. Thus, the enhanced charge extraction from perovskite to the BHJ layer is very likely to result from the charge extraction from perovskite to polymer. When laser shines on the films, both perovskite and polymer are excited since 640 nm lies in

DOI: 10.1021/acs.nanolett.7b02532
Nano Lett. 2017, 17, 5140−5147

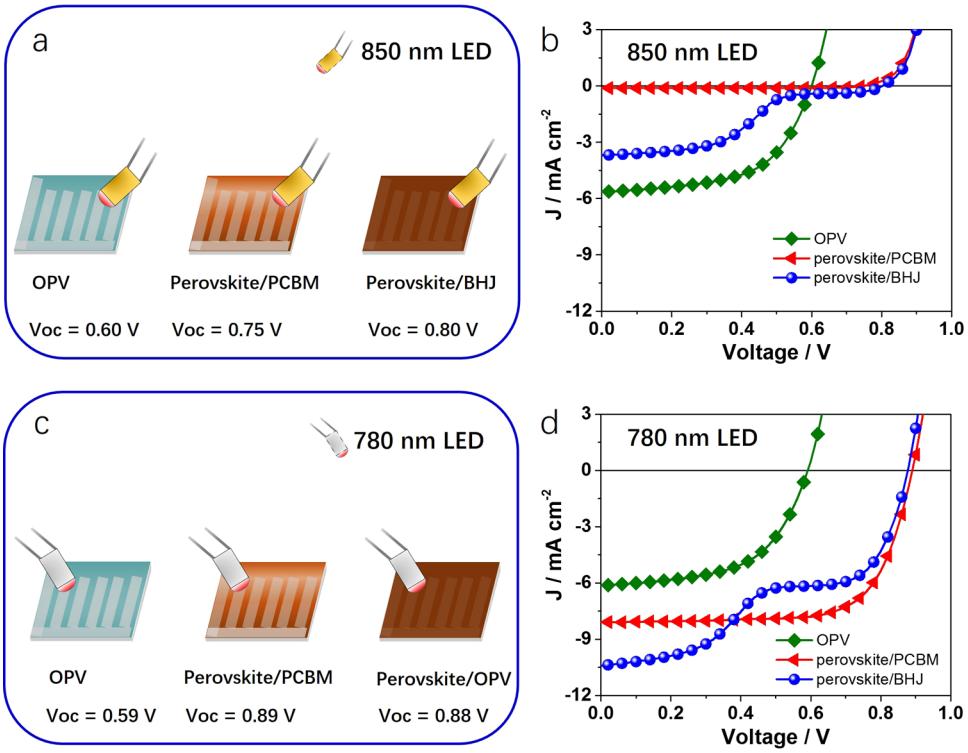

Figure 4. *J*–*V* curves of integrated perovskite/BHJ cell under illumination of monochromatic LED at wavelengths of (a,b) 850 nm, and (c, d) 780 nm.

the absorption range of both. The excitation is accompanied by splitting of E_f^n and E_f^p in the perovskite layer and quasi-Fermi alignment of perovskite with polymer and PCBM, respectively. Such quasi-Fermi level alignment, together with the resulting energy band bending, makes it possible for charge transfer from perovskite to the BHJ layer in a manner described above, which accounts for the faster PL quench for the perovskite/BHJ sample.

Some may argue that the faster PL quench may also result from extra charge carrier recombination brought about by the defect at the perovskite/BHJ. Here, we exclude such possibility by examining the charge dynamics behavior of the integrated perovskite/BHJ structure. The time-resolved PL (TRPL) decay of $MAPbI_{3-x}Cl_x$, $MAPbI_{3-x}Cl_x$/PCBM and $MAPbI_{3-x}Cl_x$/BHJ films on glass substrates, as shown in Figure 3b, were measured to compare the charge injection/separation behavior for the perovskite/PCBM and perovskite/BHJ. The decay curves have a biexponential character by fitting the data. We also used a longer lifetime for comparison. The PL decay of the perovskite/BHJ film exhibits a PL lifetime of 0.12 μs, which is shorter than that of perovskite/PCBM film (t = 0.27 μs) and neat perovskite film (t = 0.65 μs). The PL quenching in the perovskite/BHJ film was faster than that in the perovskite/PCBM film, confirming faster charge transfer from perovskite into the BHJ layer than into the PCBM film.

In addition to PL and TRPL, the carrier dynamics along the entire pathway in the completed devices were measured by laser-induced transient photocurrent (TPC) and transient photovoltage (TPV) technique.[34,35] Note that a white light bias was used to simulate 1 sun working condition for the TPC and TPV measurements. BHJ OPV device was also tested for comparison (Figure S8, Supporting Information). All the charge carrier lifetimes extracted from the photocurrent decay and photovoltage decay curves are summarized in Table 1. As shown in Figure 3c, the photocurrent decay lifetimes are 0.68 and 0.46 μs for the conventional device and integrated device, respectively. The shorter delay time of the integrated device compared with that of the conventional device indicates that the electron carrier extraction ability of BHJ layer is better than that of PCBM layer, which is consistent with the PL and TRPL results and strengthens our quasi-Fermi level pinning model. Transient photovoltage decay measurements indicate how fast injected electrons can recombine from which the charge carrier lifetime can be extracted. A fast decay of photovoltage indicates fast recombination. The lifetimes are derived from single exponential fitting of decay curves of perovskite reference and integrated devices. As shown in Figure 3d, carrier lifetime for the device based on integrated device is 0.99 μs, which is longer than that of the conventional device (0.45 μs). The results indicated that the lower charge carrier recombination velocity in the integrated device, which further attributes the faster carrier extraction of BHJ from perovskite layer to the band alignment, rather than defect-induced PL quench.

On the basis of the above analysis, the integrated perovskite/BHJ solar cell is dual-cell functioning together upon illumination. Therefore, it is of great interest to us what the situation will be if only one single layer of the perovskite/BHJ bilayer is functioning. Hence, the integrated cells were carefully encapsulated and taken out of glovebox for further investigated. From the absorption and EQE curves described above, the reference perovskite solar cell shows an onset at 800 nm. So the photoresponse of the integrated cells to the spectrum ranged beyond 800 nm is contributed by the low bandgap polymer based BHJ layer. Commercialized LED851L emits NIR light centered at 850 nm with an full width at half-maximum of 40 nm. Within this range, only the bulk-heterojunction layer of the integrated solar cell will be excited, while the perovskite layer will not. We used such monochromatic LED to excite the

DOI: 10.1021/acs.nanolett.7b02532
Nano Lett. 2017, 17, 5140–5147

integrated cells and investigate its photovoltaic behavior. In this experiment, the PDTP-DFBT:PCBM based OPV BHJ cell was also measured as a reference. The detailed solar cell performance parameters are summarized in Table S3. As shown in Figure 4b, under illumination of LED851L, the OPV cell delivers a V_{OC} of 0.60 V, a J_{SC} of 5.65 mA cm^{-2}, and an FF of 57.3%, which are all comparable to the values of OPV under 1 sun illumination. These values also confirm that the intensity of the working LED851L is strong enough to induce sufficient quasi-Fermi levels splitting in the bulk-heterojunction layer. For the integrated perovskite/BHJ solar cell shown in Figure 4a, the LED851L illumination results in a V_{OC} of 0.80 V, which is quite considerably lower than the open circuit voltage we got above from the integrated cell by 1 solar illumination. The underlined mechanism can be partially understood: LED851L will not excite the perovskite layer efficiently. When the perovskite is not "active", there is no enough excited carriers for Fermi level splitting and no quasi-Fermi level pinning as described above. The perovskite functions mainly as a transporting layer for the working OPV cell. Thus, the open circuit voltage in this case will be dominated by the OPV. Note that the perovskite still has some contribution to the Voc of perovskite/BHJ based device as the 850 nm LED light with light centered at 850 nm still has a very weak light band tail extend to 800 nm.

For a short conclusion, we believe that the quasi-Fermi level pinning is the physical origin of the high V_{OC} of the integrated perovskite/BHJ solar cell. There are certainly other side factors that will contribute to the open circuit voltage. One possible reason could be the morphological difference between PCBM and BHJ film. PCBM is a small molecule with a tendency to aggregate. Thus, the PCBM film might not be sufficient to cover the perovskite surface, which results in severe charge recombination loss on the cathode side. By blending with the polymer, the bulk heterojunction should be able to form a conformal and continuous film to separate the metal cathode and perovskite. Thus, the low charge recombination velocity in the BHJ film, as discussed before, results in a slightly higher V_{OC}.

Moreover, we believe that the unique configurational and material properties of this perovskite/BHJ structure make it possible for the quasi-Fermi level to pin to that of perovskite. This can be verified by testing the photovoltaic behavior of the devices illuminated with monochromatic LED at 780 nm. From the EQE curves, we know that perovskite will have very weak photoresponse while BHJ layer will generate considerable photoinduced carriers. In this case, the perovskite will get "thirsty" to pin the quasi-Fermi levels of the whole system and thus will not be able to dominate the open circuit voltage of the integrated cell. This can be verified by testing the photovoltaic behavior of the devices illuminated with monochromatic LED at 780 nm (Figure 4). The $J-V$ curve of integrated perovskite/BHJ solar cell under monochromatic LED at 780 nm is shown in Figure 4d. Fitted data shows that the V_{OC} of the integrated solar cell falls to 0.88 V, which is lower than that of the normally working cell under 1 solar illumination. The large V_{OC} drop confirms our claim that the great disparity in carrier concentration is crucial to the pinning of quasi-Fermi levels and thus to the preserved high V_{OC} of the integrated solar cell. In addition, the BHJ layer, which is originally aimed to enhance the perovskite solar cell performance mainly by utilizing the NIR light after perovskite's absorption cutoff at 800 nm, is a blend of two single semiconductor components. This unique character of BHJ configuration makes it possible for perovskite's E_f^n and E_f^p to simultaneously align with the E_f^n of PCBM and the E_f^p of polymer in the BHJ, respectively. To our best knowledge, materials that satisfy the above energy level requirement can hardly be identified. This can be verified in previous studies which incorporate PbS quantum dots into the perovskite solar cell as an infrared absorber as well as a charge transporting material. The output of V_{OC} is significantly lower than that of a normally working perovskite solar cell due to poor energy band alignment of quantum dot layer and perovskite layer.[36−38] We notice in the perovskite/PbS system that only one set of E_f^n and E_f^p coexist in each layer under illumination. The HOMO level of PbS reported is slightly lower than that of perovskite, so the E_f^n energy gap between the LUMO level of PbS and that of perovskite is very small, thus the large bending of valence band is needed for E_f^p alignment. Such unbalance accounts for the low V_{OC} of the integrated perovskite/PbS solar cell. At the same time, both HOMO level and LUMO level of PbS lie within the bandgap of perovskite. So when PbS is used as an electron transporting layer for perovskite, holes also move toward PbS and the device will go through huge charge carrier recombination and thus suffer severe V_{OC} loss.

In conclusion, we have demonstrated high-performance integrated perovskite/BHJ solar cells and found that the improved performance is ascribed to the low carrier recombination rate, high V_{OC} and increased light absorption ability in NIR region of integrated devices. The key finding of the present work is that the V_{OC} of the integrated device is dominated by (or pinned to) the perovskite cells, not the OPV cells. We showed for the first time a quasi-Fermi Level Pinning Model to understand the working principles of this integrated device and to demonstrate the physical origin of the V_{OC} of the integrated perovskite/BHJ solar cell. The V_{OC} of the integrated cell is determined by the quasi-Fermi level splitting of the biabsorption layer system, which are pinned to that of the perovskite layer. Such quasi-Fermi level pinning is an outcome of the uniqueness of the perovskite/BHJ configuration and distinct material properties of the two layers and accounts for the fact that perovskite, the one which delivers higher V_{OC} of the two layers, dominates the open circuit voltage of the integrated solar cell. It should be noted that the Fermi energy pinning model is one of the models we have to explain the abnormal large V_{OC} in this type of solar cells, while it does not exclude other possible models which is still in the development. On the basis of our findings, the integrated device always provides additional light harvesting in the NIR without sacrificing V_{OC}; more enhanced PCEs of 20% or higher are expected by integrating more efficient perovskite layers with the optimized NIR polymer-based BHJ layers, thus paving a new way to further enhance the performance of perovskite solar cells and suggesting a new direction to high-performance photovoltaic device for future industry application.

■ ASSOCIATED CONTENT

Supporting Information

The Supporting Information is available free of charge on the ACS Publications website at DOI: 10.1021/acs.nanolett.7b02532.

Detailed experimental procedures (PDF)

DOI: 10.1021/acs.nanolett.7b02532
Nano Lett. 2017, 17, 5140−5147

AUTHOR INFORMATION

Corresponding Authors

*E-mail: (Y.L.) liuys@nankai.edu.cn.
*E-mail: (Y.Y.) yangy@ucla.edu.

ORCID

Jinsong Huang: 0000-0002-0509-8778
Yang Yang: 0000-0001-8833-7641

Author Contributions

The manuscript was written through contributions of all authors. All authors have given approval to the final version of the manuscript. S.Q. and Y.L. contributed equally to this work.

Notes

The authors declare no competing financial interest.

ACKNOWLEDGMENTS

This work was financially supported by a grant from the Office of Naval Research (Grant N00014-17-1-2484 and N00014-14-1-0648) and by the Air Force Office of Scientific Research (Grant FA2386-15-1-4108). Y.L. thanks the financial support from National Natural Science Foundation of China (Grant 51673097 and 91633301). Z.H. thanks Dr. Chunjun Liang from Beijing Jiaotong University for valuable discussion and critical comments on energy level alignment in photovoltaic cells. J.H. thanks the financial support from National Science Foundation (Grant ECCS-1252623). We thank Professor Eli Yablonovitch of UC Berkeley and Daniel Friedman of NREL for technical discussions. The authors sincerely acknowledge Mr. Nicholas De Marco and Mr. Onur Sahin for their help with English editing and the Enli Tech (in Taiwan) for donating the EQE measurement system to UCLA.

REFERENCES

(1) Chen, Q.; De Marco, N.; Yang, Y.; Song, T. B.; Chen, C. C.; Zhao, H. X.; Hong, Z. R.; Zhou, H. P.; Yang, Y. *Nano Today* **2015**, *10*, 355−396.
(2) Jung, H. S.; Park, N. G. *Small* **2015**, *11*, 10−25.
(3) Kojima, A.; Teshima, K.; Shirai, Y.; Miyasaka, T. *J. Am. Chem. Soc.* **2009**, *131*, 6050−6051.
(4) Kim, H. S.; Lee, C. R.; Im, J. H.; Lee, K. B.; Moehl, T.; Marchioro, A.; Moon, S. J.; Humphry-Baker, R.; Yum, J. H.; Moser, J. E.; Gratzel, M.; Park, N. G. *Sci. Rep.* **2012**, *2*, 591.
(5) Yang, W. S.; Noh, J. H.; Jeon, N. J.; Kim, Y. C.; Ryu, S.; Seo, J.; Seok, S. I. *Science* **2015**, *348*, 1234−1237.
(6) Yi, C. Y.; Li, X.; Luo, J. S.; Zakeeruddin, S. M.; Gratzel, M. *Adv. Mater.* **2016**, *28*, 2964−2970.
(7) Zhou, H. P.; Chen, Q.; Li, G.; Luo, S.; Song, T. B.; Duan, H. S.; Hong, Z. R.; You, J. B.; Liu, Y. S.; Yang, Y. *Science* **2014**, *345*, 542−546.
(8) Gratzel, M. *Nat. Mater.* **2014**, *13*, 838−842.
(9) Stranks, S. D.; Eperon, G. E.; Grancini, G.; Menelaou, C.; Alcocer, M. J. P.; Leijtens, T.; Herz, L. M.; Petrozza, A.; Snaith, H. J. *Science* **2013**, *342*, 341−344.
(10) Xing, G. C.; Mathews, N.; Sun, S. Y.; Lim, S. S.; Lam, Y. M.; Gratzel, M.; Mhaisalkar, S.; Sum, T. C. *Science* **2013**, *342*, 344−347.
(11) Li, G.; Zhu, R.; Yang, Y. *Nat. Photonics* **2012**, *6*, 153−161.
(12) You, J. B.; Dou, L. T.; Hong, Z. R.; Li, G.; Yang, Y. *Prog. Polym. Sci.* **2013**, *38*, 1909−1928.
(13) Hagfeldt, A.; Boschloo, G.; Sun, L. C.; Kloo, L.; Pettersson, H. *Chem. Rev.* **2010**, *110*, 6595−6663.
(14) Gratzel, M. *Acc. Chem. Res.* **2009**, *42*, 1788−1798.
(15) Wang, J. Y.; Liu, K.; Ma, L. C.; Zhan, X. W. *Chem. Rev.* **2016**, *116*, 14675−14725.
(16) Cheng, P.; Zhan, X. W. *Chem. Soc. Rev.* **2016**, *45*, 2544−2582.
(17) Docampo, P.; Bein, T. *Acc. Chem. Res.* **2016**, *49*, 339−346.
(18) Gao, P.; Gratzel, M.; Nazeeruddin, M. K. *Energy Environ. Sci.* **2014**, *7*, 2448−2463.
(19) Lin, Y. Z.; Shen, L.; Dai, J.; Deng, Y. H.; Wu, Y.; Bai, Y.; Zheng, X. P.; Wang, J. Y.; Fang, Y. J.; Wei, H. T.; Ma, W.; Zeng, X. C.; Zhan, X. W.; Huang, J. S. *Adv. Mater.* **2017**, *29*, 1604545.
(20) Zhang, M. Y.; Li, T. F.; Zheng, G. H. J.; Li, L.; Qin, M.; Zhang, S. M.; Zhou, H. P.; Zhan, X. W. *Mater. Chem. Front* **2017**, DOI: 10.1039/C7QM00221A.
(21) Hao, F.; Stoumpos, C. C.; Cao, D. H.; Chang, R. P. H.; Kanatzidis, M. G. *Nat. Photonics* **2014**, *8*, 489−494.
(22) Stoumpos, C. C.; Malliakas, C. D.; Kanatzidis, M. G. *Inorg. Chem.* **2013**, *52*, 9019−9038.
(23) Ogomi, Y.; Morita, A.; Tsukamoto, S.; Saitho, T.; Fujikawa, N.; Shen, Q.; Toyoda, T.; Yoshino, K.; Pandey, S. S.; Ma, T. L.; Hayase, S. *J. Phys. Chem. Lett.* **2014**, *5*, 1004−1011.
(24) Hao, F.; Stoumpos, C. C.; Chang, R. P. H.; Kanatzidis, M. G. *J. Am. Chem. Soc.* **2014**, *136*, 8094−8099.
(25) Shockley, W.; Queisser, H. J. *J. Appl. Phys.* **1961**, *32*, 510−519.
(26) Liu, Y. S.; Hong, Z. R.; Chen, Q.; Chang, W. H.; Zhou, H. P.; Song, T. B.; Young, E.; Yang, Y.; You, J. B.; Li, G.; Yang, Y. *Nano Lett.* **2015**, *15*, 662−668.
(27) Zuo, C. T.; Ding, L. M. *J. Mater. Chem. A* **2015**, *3*, 9063−9066.
(28) Kim, J.; Kim, G.; Back, H.; Kong, J.; Hwang, I. W.; Kim, T. K.; Kwon, S.; Lee, J. H.; Lee, J.; Yu, K.; Lee, C. L.; Kang, H.; Lee, K. *Adv. Mater.* **2016**, *28*, 3159−3165.
(29) You, J. B.; Dou, L. T.; Yoshimura, K.; Kato, T.; Ohya, K.; Moriarty, T.; Emery, K.; Chen, C. C.; Gao, J.; Li, G.; Yang, Y. *Nat. Commun.* **2013**, *4*, 1446.
(30) Dou, L. T.; You, J. B.; Yang, J.; Chen, C. C.; He, Y. J.; Murase, S.; Moriarty, T.; Emery, K.; Li, G.; Yang, Y. *Nat. Photonics* **2012**, *6*, 180−185.
(31) Berry, J.; Buonassisi, T.; Egger, D. A.; Hodes, G.; Kronik, L.; Loo, Y. L.; Lubomirsky, I.; Marder, S. R.; Mastai, Y.; Miller, J. S.; Mitzi, D. B.; Paz, Y.; Rappe, A. M.; Riess, I.; Rybtchinski, B.; Stafsudd, O.; Stevanovic, V.; Toney, M. F.; Zitoun, D.; Kahn, A.; Ginley, D.; Cahen, D. *Adv. Mater.* **2015**, *27*, 5102−5112.
(32) Unger, E. L.; Hoke, E. T.; Bailie, C. D.; Nguyen, W. H.; Bowring, A. R.; Heumuller, T.; Christoforo, M. G.; McGehee, M. D. *Energy Environ. Sci.* **2014**, *7*, 3690−3698.
(33) Zhao, Y. X.; Zhu, K. *Chem. Soc. Rev.* **2016**, *45*, 655−689.
(34) Chen, Q.; Zhou, H. P.; Fang, Y. H.; Stieg, A. Z.; Song, T. B.; Wang, H. H.; Xu, X. B.; Liu, Y. S.; Lu, S. R.; You, J. B.; Sun, P. Y.; Mckay, J.; Goorsky, M. S.; Yang, Y. *Nat. Commun.* **2015**, *6*, 7269.
(35) Xiao, Z. G.; Dong, Q. F.; Bi, C.; Shao, Y. C.; Yuan, Y. B.; Huang, J. S. *Adv. Mater.* **2014**, *26*, 6503−6509.
(36) Etgar, L.; Gao, P.; Qin, P.; Graetzel, M.; Nazeeruddin, M. K. *J. Mater. Chem. A* **2014**, *2*, 11586−11590.
(37) Li, Y.; Zhu, J.; Huang, Y.; Wei, J. F.; Liu, F.; Shao, Z. P.; Hu, L. H.; Chen, S. H.; Yang, S. F.; Tang, J. W.; Yao, J. X.; Dai, S. Y. *Nanoscale* **2015**, *7*, 9902−9907.
(38) Liu, C.; Wang, K.; Du, P. C.; Wang, E. M.; Gong, X.; Heeger, A. J. *Nanoscale* **2015**, *7*, 16460−16469.

DOI: 10.1021/acs.nanolett.7b02532
Nano Lett. 2017, 17, 5140−5147